Microseismic event estimation in noisy data via full waveform inversion

Jordan Kaderli, Matthew D. McChesney, and Susan E. Minkoff, The University of Texas at Dallas*

SUMMARY

Full waveform inversion accurately estimates the full spatial and temporal description of a microseismic source which includes not only the location and origin time of the source but also the waveform itself. Assuming two-dimensional acoustic wave propagation, the gradient is computed via the adjoint-state method for both the spatial radiation pattern and the temporal waveform of the source. Neither of these gradients requires storing the forward solution of the wave equation as is required by the imaging condition for velocity inversion. This approach identifies multiple sources, handles extremely low signal-to-noise ratio data, and produces accurate results in the absence of a good initial estimate.

INTRODUCTION

Hydraulic fracturing is used to enable extraction of oil and gas from low permeability materials such as shale. In hydraulic fracturing, liquid is injected into the well under high pressure to create fractures thereby allowing the oil and gas to flow more freely. The propagation of these fractures causes stress changes in the rock that may result in the emission of energy in the form of microseismic events. Identification of the source parameters of these microseismic events provides a means of quantifying the extent and effectiveness of the hydraulic stimulation. As such, determining the locations and origin times of microseismic sources has become an important area of research in exploration seismology. Traditional methods for locating microseismic events include P-wave and S-wave travel-time analysis (Eisner et al. (2009); Zhebel and Eisner (2015)), hodogram analysis (Han et al. (2009)), and travel-time inversion (Maxwell (2014)). One disadvantage of all of these methods is susceptibility to noise; in particular, travel-time analysis requires one to visually pick the first arrivals of the wavefields emitted by the microseismic event, which can be impossible in noisy data. In addition to more traditional methods, imaging and inversion techniques have been used to determine source parameters. Minkoff and Symes (1997) use full waveform inversion (FWI) to invert for both the mechanical earth parameters and the seismic source assuming the source location is known. Ramos-Martinez and McMechan (2001) estimate source parameters via FWI in viscoelastic, anisotropic media, assuming an *a priori* estimate of both the source location and the source time function. Wu and McMechan (1996) use FWI to determine the spatial coordinates x_s and z_s and origin time t_0 as well as the amplitude and angle associated with the double-couple assuming a known source time function and elastic wave propagation. Jarillo Michel and Tsvankin (2014a,b) use FWI to invert for the spatial coordinates $\mathbf{x}_s$ and origin time t_0 as well as the moment-tensor of the source assuming a very good initial estimate of the source location. Xuan and Sava (2010) use time reversal methods in the context of Bayesian inversion theory to estimate the source location from data with noise, assuming some *a priori* knowledge of the true source. Artman et al. (2010); Artman and Witten (2011) use time-reverse imaging to locate microseismic events.

In this work, we use gradient-based FWI to invert for the spatial radiation pattern and the temporal waveform of the source assuming the source can be written as a separable function of space and time and the velocity is known. By inverting for the complete waveforms in space and time rather than just the location and origin time, the method is able to correctly identify multiple spatially separated sources occurring simultaneously, even when the number of sources is not known *a priori*. Furthermore, this approach produces accurate results in the absence of a good initial guess. This method has the ability to handle data with substantial amounts of noise including cases where no event is visually identifiable in the recorded data so travel-time picking of first arrivals would be impossible. Thus our work differs from previous work in that the authors mentioned above either inverted for only the source location and and origin time, required a good initial estimate of the source, were unable to handle very noisy data, or used time reversal techniques rather than gradient-based inversion.

THEORY

We model wave propagation through a constant density medium using the two-dimensional acoustic wave equation:

$$m(x,z)\frac{\partial^2 u(x,z,t)}{\partial t^2} - \nabla^2 u(x,z,t) = f(x,z)\,w(t) \qquad (1)$$

where $m(x,z)$ is the known squared slowness, i.e. $m = 1/c^2$ where c is the sound velocity, $f(x,z)$ and $w(t)$ are the spatial and temporal components of the source of acoustic energy, respectively, and $u(x,z,t)$ is the acoustic pressure. We use FWI to invert for both $f(x,z)$ and $w(t)$.

We will describe 3 sets of experiments. In the first set of experiments we consider the case where $w(t)$ is a known Ricker wavelet, and we invert only for the spatial component $f(x,z)$. To determine f, we minimize the least squares objective functional $J(f) = \frac{1}{2}\|d_{pred} - d_{obs}\|^2$, where d_{pred} is the data generated by solving the wave equation with our current estimate of the source, and d_{obs} is the data recorded at the receivers. To minimize the objective functional, we use a gradient descent algorithm, (e.g. the conjugate gradient method). Using the adjoint-state method, we compute the gradient to be

$$D_f J(x,z) = \int_0^T w(t)\,\lambda(x,z,t)\,dt$$

where λ is the solution to the adjoint equation. In contrast, the gradient for the velocity inversion problem is well known to be

$$D_m J(x,z) = -\int_0^T \frac{\partial^2 u(x,z,t)}{\partial t^2}\lambda(x,z,t)\,dt$$

DOI http://dx.doi.org/10.1190/segam2015-5867154.1

(Gunzburger (2003); Oberai et al. (2003); Plessix (2006)). The gradient for velocity inversion requires one to store the solution to both the forward problem and the time-reversed adjoint problem (Symes (2007)), whereas the gradient for source inversion does not. Thus, there is no need for checkpointing in the source inversion problem.

In the second set of experiments, we consider the case where $f(x,z)$ is known, and we invert only for the time-dependent wavelet $w(t)$. In that case, we must minimize the least squares objective functional $J(w) = \frac{1}{2}\|d_{pred} - d_{obs}\|^2$ using the corresponding gradient

$$D_w J(t) = \int_\Omega f(x,z)\,\lambda(x,z,t)\,dx\,dz.$$

In the final experiment, we invert for both the spatial and temporal components of the source using coordinate search or alternation (Minkoff and Symes (1997)) as follows:

1. Given the current spatial component of the source $f_c(x,z)$ and current wavelet $w_c(t)$, invert for an improved estimate $f_+(x,z)$.
2. Replace $f_c(x,z)$ by $f_+(x,z)$.
3. Given the current spatial component $f_c(x,z)$ and current wavelet $w_c(t)$, invert for an improved estimate of the wavelet $w_+(t)$.
4. Replace $w_c(t)$ by $w_+(t)$.
5. Repeat Steps 1 through 4 until convergence.

The inversion algorithm was implemented in PySIT, an open source toolbox for seismic inversion written in Python by the Imaging and Computing Group at MIT (Hewett (2011)). The open source version of PySIT performs velocity inversion assuming a known source of acoustic energy. The modified version used in this work performs source inversion assuming a known velocity. All experimental results shown in this work were performed on a single processor laptop. While the numerical results described here were produced by minimizing the standard least squares objective functional, we also performed a number of simulations involving a Tikhonov-regularized version of the objective functional which reduced the impact of the initial guess on subsequent estimates (Hansen (1998)).

NUMERICAL RESULTS

In the first set of numerical experiments, we assume the wavelet $w(t)$ is known and invert for the spatial component of the source $f(x,z)$. In all experiments shown, we assume a known constant velocity medium. The mesh contains 181 x 141 grid points, and there are two spatially separated sources, located at $(x,z) = (.4,.3)$ and $(x,z) = (.7,.3)$. The experimental setup is shown in Figure 1. The temporal component $w(t)$ is a 20 Hz Ricker wavelet. We take our initial guess for $f(x,z)$ to be zero everywhere, i.e. no *a priori* knowledge of the source locations or number of sources is assumed. The recorded data generated by the two sources is shown in Figure 2. Figure 3 shows that the true sources are correctly identified after a single iteration of inversion.

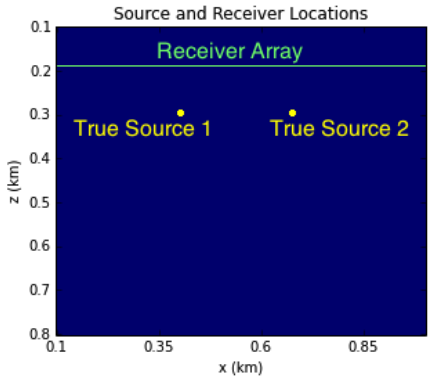

Figure 1: Experimental configuration for the first set of numerical experiments in which the wavelet $w(t)$ is known and only the spatial component of the source $f(x,z)$ is estimated.

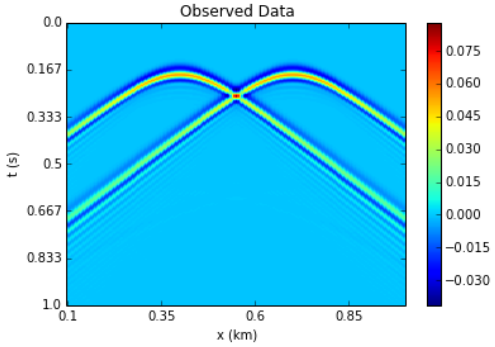

Figure 2: Recorded data for the experiment shown in Figure 1 in which the wavelet $w(t)$ is known and only the spatial component $f(x,z)$ is estimated.

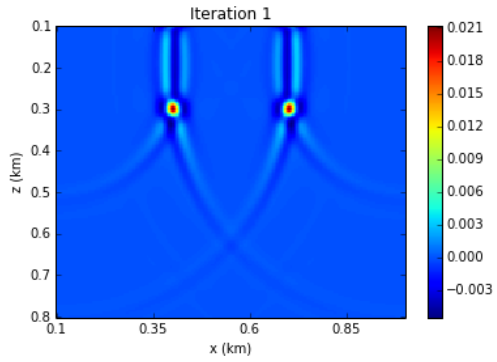

Figure 3: Estimate of the sources shown in Figure 1 after 1 iteration of FWI using the data shown in Figure 2.

The second numerical experiment is the same as the first except that we added uniformly distributed random noise to the recorded data to produce data with a .008 signal-to-noise ratio, as measured via the RMS amplitudes ratio (see Figure 4). Because the signal-to-noise ratio is so low, no event is discernible

DOI http://dx.doi.org/10.1190/segam2015-5867154.1

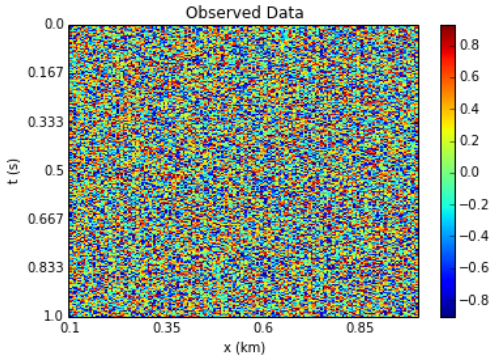

Figure 4: Recorded data with a signal-to-noise ratio of .008.

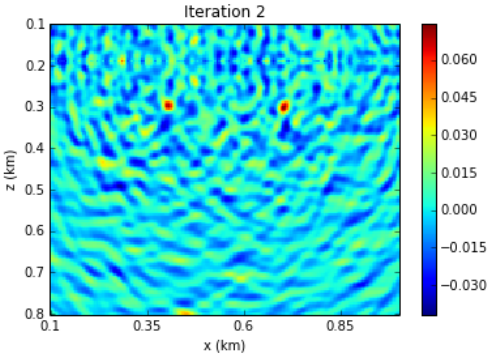

Figure 5: Estimate of the source after 2 iterations of FWI using the noisy data shown in Figure 4.

in the data. However, even in this case, the inversion algorithm correctly identifies both sources after 2 iterations (see Figure 5).

In the second set of numerical experiments, we assume the spatial component of the source $f(x,z)$ is known, and we invert for $w(t)$. As in the previous experiments, we assume a known constant velocity medium. We again use a 181 x 141 mesh with a single true source located at $(x,z) = (.4,.3)$. The temporal component $w(t)$ is a 20 Hz Ricker wavelet that peaks at .0675 s. We take our initial estimate of the wavelet to be the same 20 Hz Ricker shifted by .4325 s (see Figure 6). After 1 iteration, the estimated wavelet begins to resemble the true wavelet, and after 10 iterations, the estimated wavelet agrees well with the true wavelet both in amplitude and waveform (see Figures 7 and 8). In particular, the peaks of both the true and inversion-estimated wavelets occur at .0675 s, indicating that the origin time and shape of the wavelet have been identified correctly. In other experiments not shown here, we found that the algorithm correctly identifies the true wavelet whether the initial estimate of the wavelet is taken to be a Ricker of the wrong frequency, a first derivative Gaussian, or even identically zero.

Adding random noise to the recorded data to create the .083 signal-to-noise ratio data shown in Figure 9, we see that even when the recorded data is too noisy to allow picking first arrivals, the inversion algorithm still produces a reasonably accurate estimate of the wavelet. In particular, the peaks of the estimated wavelet and true wavelet agree, indicating that the origin time of the event has been correctly determined (see Figure 10).

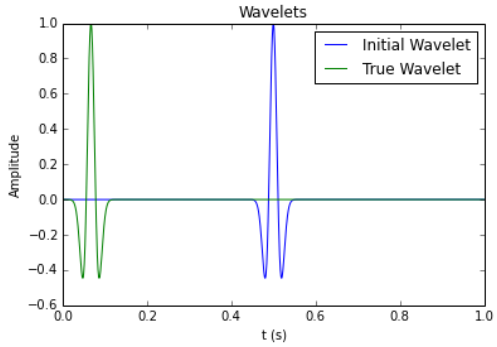

Figure 6: True and initial wavelets for the second set of experiments in which $f(x,z)$ is known and only $w(t)$ is estimated.

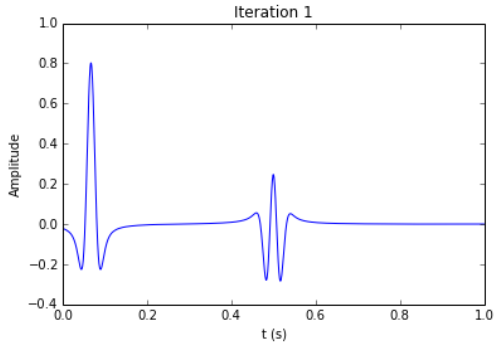

Figure 7: Estimate of the wavelet $w(t)$ after 1 iteration of FWI with $f(x,z)$ known.

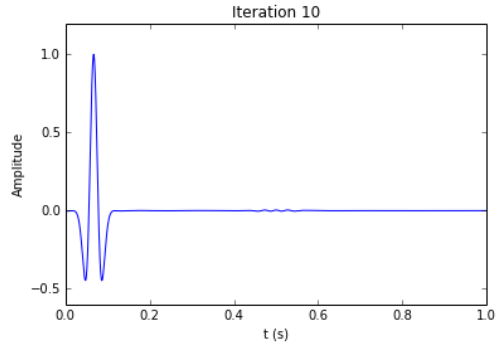

Figure 8: Estimate of the wavelet $w(t)$ after 10 iterations of FWI with $f(x,z)$ known.

Finally, we present a joint inversion for both the spatial component $f(x,z)$ and the temporal component $w(t)$ of the source. Again, the velocity is assumed constant and known, and the mesh is 181 x 141 grid points. The true source is again located at $(x,z) = (.4,.3)$. The wavelet $w(t)$ is a 20 Hz Ricker centered at .0675 s. Our initial guess for $w(t)$ is a 20 Hz Ricker wavelet

DOI http://dx.doi.org/10.1190/segam2015-5867154.1

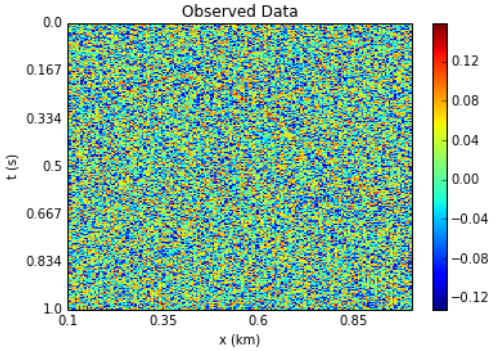

Figure 9: Recorded data with a signal-to-noise ratio of .083.

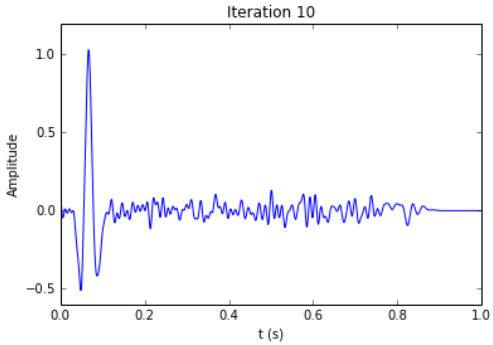

Figure 10: Estimate of $w(t)$ after 10 iterations of FWI assuming $f(x,z)$ is known and using the data shown in Figure 9.

centered at .5 s (see Figure 11). The initial guess for $f(x,z)$ is identically zero. We perform 4 iterations of inversion for $f(x,z)$ followed by 4 iterations of inversion for the wavelet. We then repeat this alternation loop 8 times. From Figures 12 and 13, one sees that in joint inversion the estimated spatial component of the source is more diffuse. However, there does exist a packet of energy centered at the true source location. Also, the estimated wavelet is noisier than in the inversion for the wavelet only. Nonetheless, the wavelet peaks near the maximum amplitude of the true wavelet. Additionally, the polarity of the spatial component of the source has flipped, and the temporal component of the source is no longer zero phase.

CONCLUSIONS

FWI accurately predicts the spatial and temporal components of the source when inverted for individually, both in the presence of significant noise and in the absence of a good initial guess. In the joint inversion case, where neither the spatial nor temporal component is known, the objective function contains multiple local minima, making it difficult to uniquely determine the source characteristics. Our approach, which produces a full description of the source in space and time, is well suited to handle source parameter estimation for microseismic events in which the energy emission is distributed across real fracture geometries and may have highly varied time dependence.

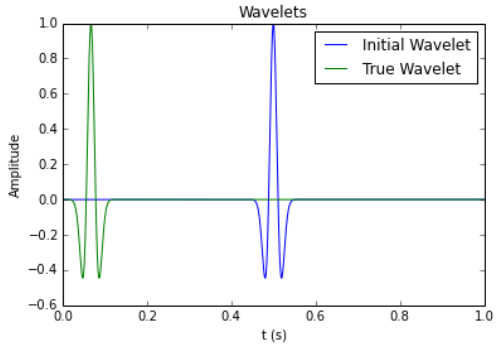

Figure 11: True and initial wavelets for the joint inversion.

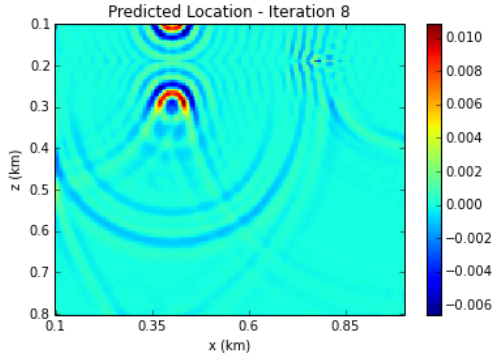

Figure 12: Estimate of the spatial component of the source after 8 iterations of joint inversion.

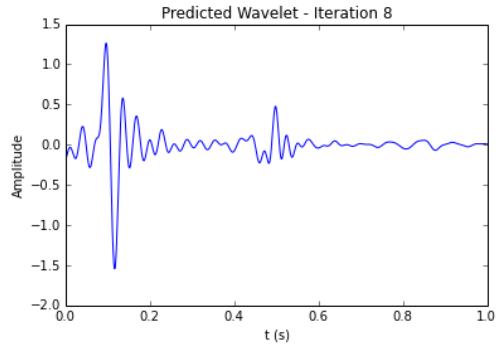

Figure 13: Estimate of $w(t)$ after 8 iterations of joint inversion.

ACKNOWLEDGMENTS

We wish to thank Pioneer Natural Resources for partially funding this project. We also wish to thank Russell J. Hewett (Total E&P Research & Technology USA.), and Het Mankad and Georgia Stuart (UTD) for their help.

DOI http://dx.doi.org/10.1190/segam2015-5867154.1

EDITED REFERENCES

Note: This reference list is a copyedited version of the reference list submitted by the author. Reference lists for the 2015 SEG Technical Program Expanded Abstracts have been copyedited so that references provided with the online metadata for each paper will achieve a high degree of linking to cited sources that appear on the Web.

REFERENCES

Artman, B., I. Podladtchikov, and B. Witten, 2010, Source location using time-reverse imaging: Geophysical Prospecting, **58**, no. 5, 861–873, http://dx.doi.org/10.1111/j.1365-2478.2010.00911.x.

Artman, B., and B. Witten, 2011, Wave-equation microseismic imaging and event selection in the image domain: 81st Annual International Meeting, SEG, Expanded Abstracts, 1699–1703.

Eisner, L., P. Duncan, W. Heigl, and W. Keller, 2009, Uncertainties in passive seismic monitoring: The Leading Edge, **28**, 648–655, http://dx.doi.org/10.1190/1.3148403.

Gunzburger, M. D., 2003, Perspectives in flow control and optimization: SIAM.

Han, L., J. Wong, and J. C. Bancroft, 2009, Hypocenter location using hodogram analysis of noisy 3C microseismograms: Consortium for Research in Elastic Wave Exploration Seismology (CREWES) Research Report 29, http://www.crewes.org/ForOurSponsors/ResearchReports/2009/CRR200929.pdf.

Hansen, P. C., 1998, Rank-deficient and discrete ill-posed problems: Numerical aspects of linear inversion: SIAM, http://dx.doi.org/10.1137/1.9780898719697.

Hewett, R. J., and L. Demanet, 2011, PySIT: Seismic imaging toolbox for Python: Massachusetts Institute of Technology/PySIT Development, pysit.bitbucket.org.

Jarillo Michel, O., and I. Tsvankin, 2014a, Gradient calculation for waveform inversion of microseismic data in VTI media: Journal of Seismic Exploration, **23**, no. 3, 201–217.

Jarillo Michel, O., and I. Tsvankin, 2014b, Waveform inversion for parameters of microseismic sources in VTI media: 84th Annual International Meeting, SEG, Expanded Abstracts, 1045–1048.

Maxwell, S., 2014, Microseismic imaging of hydraulic fracturing: Improved engineering of unconventional shale reservoirs: SEG.

Minkoff, S., and W. Symes, 1997, Full waveform inversion of marine reflection data in the plane wave domain: Geophysics, **62**, 540–553, http://dx.doi.org/10.1190/1.1444164.

Oberai, A. A., N. H. Gokhale, and G. R. Feijóo, 2003, Solution of inverse problems in elasticity imaging using the adjoint method: Inverse Problems, **19**, no. 2, 297–313, http://dx.doi.org/10.1088/0266-5611/19/2/304.

Plessix, R., 2006, A review of the adjoint-state method for computing the gradient of a functional with geophysical applications: Geophysical Journal International, **167**, no. 2, 495–503, http://dx.doi.org/10.1111/j.1365-246X.2006.02978.x.

Ramos-Martinez, J., and G. A. McMechan, 2001, Source parameter estimation by full waveform inversion in 3D heterogeneous, viscoelastic, anisotropic media: Bulletin of the Seismological Society of America, **91**, no. 2, 276–291, http://dx.doi.org/10.1785/0120000017.

Symes, W., 2007, Reverse time migration with optimal checkpointing: Geophysics, **72**, no. 5, SM213–SM222, http://dx.doi.org/10.1190/1.2742686.

Wu, Y., and G. A. McMechan, 1996, Elastic full-waveform inversion for earthquake source parameters: Geophysical Journal International, **127**, no. 1, 61–74, http://dx.doi.org/10.1111/j.1365-246X.1996.tb01535.x.

Xuan, R., and P. Sava, 2010, Probabilistic microearthquake location for reservoir monitoring: Geophysics, **75**, no. 3, MA9–MA26, http://dx.doi.org/10.1190/1.3417757.

Zhebel, O., and L. Eisner, 2015, Simultaneous microseismic event localization and source mechanism determination: Geophysics, **80**, no. 1, KS1–KS9, http://dx.doi.org/10.1190/geo2014-0055.1.